Algorithms to Identify Detector Compton Scatter in PET Modules*

K. A. Comanor, P. R. G. Virador and W. W. Moses
Lawrence Berkeley Laboratory, University of California, Berkeley, CA 94720

Abstract

Using Monte Carlo simulation, we investigate algorithms to identify and correct for detector Compton scatter in hypothetical PET modules with 3x3x30 mm BGO crystals coupled to individual photosensors. Rather than assume a particular design, we study three classes of detectors: (1) with energy resolution limited by counting statistics, (2) with energy resolution limited by electronic noise, and (3) with depth of interaction (DOI) measurement capability. For the first two classes, selecting the channel with the highest signal as the crystal of interaction yields a 22–25% misidentification fraction (MIF) for all reasonable noise fwhm to signal (N/S) ratios (*i.e.* <0.5 at 511 keV). Algorithms that attempt to correctly position events that undergo forward Compton scatter using only energy information can reduce the MIF to 12%, and can be easily realized with counting statistics limited detectors but can only be achieved with very low noise values for noise limited detectors. When using position of interaction to identify forward scatter, a MIF of 12% can be obtained if the detector has good energy and position resolution.

I. INTRODUCTION

The use of PET in medical research has stimulated development of detectors with improved spatial resolution. One factor that degrades the performance of these designs is crystal misidentification caused by detector Compton scatter. By examining the signature of Compton scatter events, we seek to identify and correct for detector scatter by improving the ability to determine the crystal of first interaction, and hence improve the accuracy of the reconstructed image.

Several recent proposals for high resolution PET detector modules incorporate small scintillation crystals that are individually coupled to photosensors [1–3]. Earlier work suggests that such designs could identify and reject events that Compton scatter in the detector ring, thereby improving image accuracy [4] but greatly reducing sensitivity. This paper extends the previous work by developing algorithms that identify detector Compton scatter and assign events to the detector element where the first interaction occurred, thereby improving the accuracy with no loss in sensitivity. Rather than assume a particular design, we study three classes of detectors: those with energy resolution limited by counting statistics (such as conventional scintillator / PMT designs) [1, 3], those with energy resolution limited by an energy independent electronic noise (such as PIN photodiode based designs) [2], and those capable of measuring the interaction depth in the crystal [5–7].

*This work supported in part by the U.S. Department of Energy under Contract DE-AC-76SF00098, in part by the National Institutes of Health under grants P01-HL25840 and R01-NS29655.

II. MONTE CARLO SIMULATION METHODS

Individual detectors are modeled as 3x3x30 mm BGO scintillator crystals arranged in an 8x8 array which defines a module. Each crystal is coupled to an individual photosensor and modules are arranged in a 60 cm diameter, 2.4 cm axial extent PET ring. For each data point 25,000 positron annihilations are simulated (with both annihilation photons impinging on the detector ring), so all results have a 0.6% rms statistical uncertainty. Energy dependent Compton and photoelectric cross sections are used to track the location and amount of energy deposit in each detector crystal until the photon escapes from the PET ring or photoelectric absorption occurs. The true crystal of first interaction is determined by the simulation for eventual comparison with the crystal identified by a given algorithm. Events are rejected if the total energy deposit in a module is less than 200 keV. Detector modules with energy resolution limited by electronic noise and those capable of depth measurement include an energy resolution contribution from counting statistics equivalent to 12% fwhm at 511 keV. While this value is optimistic, the results will be shown to be insensitive to energy resolution degradation due to counting statistics. While a multi-layer PET camera is simulated, 2-D reconstruction using a sharp (Ra-La) filter is used.

The goal of this work is to study detector Compton scatter, so penetration effects are minimized by simulating a line source near (1 cm from) the ring's center and perpendicular to the imaging plane. An event is *misidentified* if its assigned crystal of interaction is different from the crystal of first interaction (rather than the crystal which the 511 keV photon first traverses). No "patient" scatter is simulated.

Algorithm performance is evaluated with three figures of merit: 1) the Singles Efficiency (EFF), defined as the number of events an algorithm assigns a crystal of interaction (correctly or otherwise) divided by the total number of events generated (this includes inefficiencies caused by the photon traversing the detector ring without interacting), 2) the Misidentification Fraction (MIF), defined as the number of misidentified events divided by the number of events in which an algorithm assigns a crystal of interaction, and 3) a region of interest (ROI) analysis of the reconstructed image that plots the relative activity in circular regions of interest (centered at the line source) as a function of the region radius. Like patient Compton scatter, detector Compton scatter affects quantitation more than spatial resolution, so the ROI analysis investigates spillover into regions close to the source. The ideal algorithm has high EFF, low MIF and a steep rise in the ROI curve.

III. ALGORITHMS

All algorithms begin by identifying events with detector Compton scatter. A threshold on the measured energy is

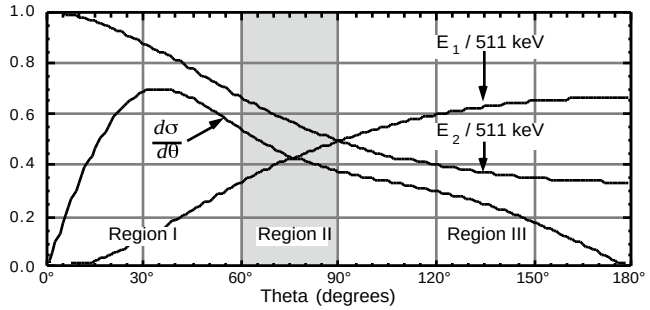

Figure 1: Compton scatter kinematics for 511 keV photons, including cross section, energy deposited at the initial interaction point (E_1) and energy carried off by the scattered photon (E_2) as a function of scattering angle.

applied to each crystal to identify those presumed to have energy deposited in them. If only one crystal is above threshold, all algorithms select it as the "correct" crystal. If more than one crystal is above threshold, all algorithms attempt to select the "correct" crystal from the crystals with the two highest measured energies. With this crystal size, the probability for a 511 keV interaction to deposit energy in one, two, and more than two crystals is 70%, 24%, and 6% respectively.

All algorithms attempt to exploit the fact that energy and momentum conservation require the energy of the scattered photon to be $511/(2-\cos\theta)$, where θ is the scattering angle (Figure 1). If E_1 is the energy deposited at the interaction point and E_2 the energy of the scattered photon (which is assumed to deposit all of its energy at another location), this relationship implies that there are three kinematic regions: Region I) Unambiguous forward scatter. When $\theta<60^\circ$, $E_1 < E_2$ and there is no value θ' that yields energies E_1' and E_2' such that $E_1' = E_2$ (and $E_2' = E_1$). Therefore, the crystal of first interaction can be unambiguously determined from the energy values alone. Region II) Ambiguous forward scatter. When $60^\circ<\theta<90^\circ$, $E_1 < E_2$ but there is a θ' such that $E_1' = E_2$ (and $E_2' = E_1$). Therefore, the crystal of first interaction cannot be unambiguously determined from the energy values alone, as backwards scatter (*i.e.* events from Region III) produces events that yield identical energy deposits. Region III) Backwards scatter (always ambiguous). When $\theta>90^\circ$, $E_1 > E_2$ but there always is a value θ' such that $E_1' = E_2$, thus the crystal of first interaction cannot be unambiguously determined from the energy values alone (*i.e.* forward scatter from Region II produces events that yield identical energy deposits).

Compton kinematics at 511 keV (also shown in Figure 1) dictate that the relative populations in Region I, II, and III are 50%, 20%, and 30% respectively. However, many of the events that scatter near 0° or 180° result in the scattered photon interacting (and depositing its energy) in the same crystal as the initial interaction, mimicking an initial photoelectric interaction. If we exclude these events and redefine E_1 and E_2 in terms of energy deposit in crystals (*i.e.* E_1 is the total energy deposit in the crystal of first interaction and E_2 is the total energy deposit in the crystal that absorbs the scattered photon), then the fraction of events in each of these kinematic regions (using the energy deposit in crystals) is roughly equal.

A. Maximum Signal Algorithm

The simplest algorithm implemented is the *Maximum Signal* algorithm, which selects the channel with the largest measured energy deposit as the crystal of first interaction, rejecting events where the maximum signal is below an energy threshold. All other algorithms are compared to it since it best models the techniques currently used to identify crystals with individually coupled photomultiplier tubes. This algorithm has a theoretical minimum MIF of 19%, assuming that half of the interactions that result in energy deposit in more than two crystals are misidentified. It should correctly identify those events with energy deposit in a single crystal (70%), 1/3 of the events with energy deposit in two crystals (those in kinematic Region III, which comprise 24%•1/3=8% of the events), and half from >2 crystal interactions (6%•1/2=3%). Note that by randomly selecting a crystal in events with energy deposit in two crystals, we obtain a lower theoretical minimum MIF of 15% (70% + 24%•1/2 + 3% correctly identified).

B. Reject Multiples Algorithm

The *Reject Multiples* algorithm eliminates Compton interactions by rejecting events with two or more signals above an energy threshold. It often has low efficiency but its theoretical minimum MIF is 0%, as it rejects all Compton scatters that deposit energy in more than one crystal.

C. Second Highest Signal Algorithm

The *Second Highest Signal* algorithm attempts to maintain high detection efficiency by correctly positioning Compton interaction events. It selects the channel with the smallest signal when two signals are above the energy threshold and has a theoretical minimum MIF of 11%. It correctly identifies events with energy deposit in a single crystal (70%), 2/3 of the events with energy deposit in two crystals (those in kinematic Regions I & II, which comprise 24%•2/3 = 16% of the events), and half from >2 crystal interactions (6%•1/2=3%).

D. Joint Algorithm

As we shall show, the *Maximum Signal* and *Second Highest Signal* algorithms perform well when the N/S ratio is high and low respectively. The *Joint* algorithm is a hybrid of these two algorithms which compares the difference between the highest and second highest signals EDIFF to a second threshold δ. The crystal with the second highest signal is chosen if EDIFF$<\delta$, otherwise the crystal with the highest signal is selected. For low N/S ratios, a large value of δ is used which makes the algorithm act like the *Second Highest Signal* algorithm. For high N/S ratios, a small value of δ is used which makes it act like the *Maximum Signal* algorithm. We shall show that this algorithm performs better than either the *Maximum Signal* or the *Second Highest Signal* for intermediate N/S ratios. Its theoretical minimum MIF lies somewhere between that of the *Maximum Signal* algorithm (19%) and *Second Highest Signal* algorithm (11%).

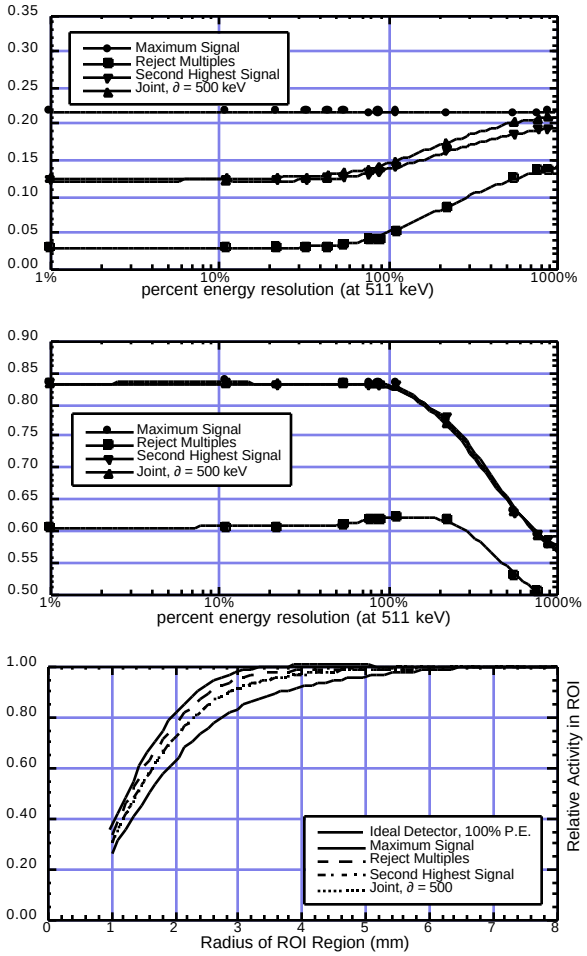

Figure 2: The (a) MIFs, (b) singles detection efficiency, and (c) relative activity in circular ROIs for each algorithm for detectors with energy resolution limited by counting statistics. Results are plotted as a function of energy resolution at 511 keV. The *Second Highest* algorithm and the *Joint* algorithm curves are overlain in (c).

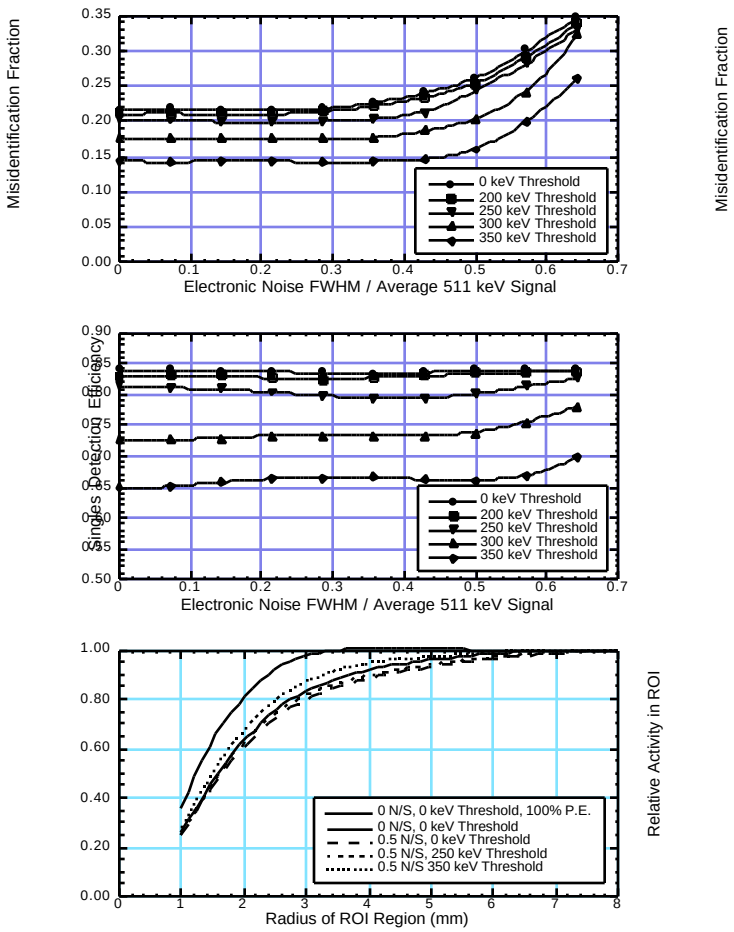

Figure 3: The (a) MIFs, (b) singles detection efficiency, and (c) relative activity in circular ROIs as a function of the region radius obtained when the *Maximum Signal* algorithm is implemented in detectors with energy resolution dominated by electrical noise.

IV. Detectors Limited by Counting Statistics

The performance of these algorithms in detectors with energy resolution limited by counting statistics (*i.e.* $\sqrt{N}$) is summarized in Figure 2. These detectors have no electronic noise, so the optimal threshold for identifying events with energy in multiple crystals is 0 keV. Figure 2a shows that for energy resolutions less than 100%, the MIFs are 22% for the *Maximum Signal* algorithm, 12% for both the *Joint* and *Second Highest Signal* algorithms, and 3% for the *Reject Multiples* algorithm. The *Joint* and the *Second Highest Signal* algorithms improve upon the *Maximum Signal* algorithm by correctly assigning forward scatter events which the latter algorithm misidentifies. The *Reject Multiples* algorithm further improves the MIF by rejecting Compton interactions, but has a low EFF (Figure 2b). All algorithms have a MIF close to their theoretical limit, indicating that noise due to counting statistics does not significantly affect these algorithms.

Figure 2c plots the relative activity in a circular region of interest (ROI) as a function of the region radius. A "perfect" detector (zero electronic noise, zero keV threshold, and a scintillator with 100% photoelectric fraction) has a steep rise in the relative activity with increasing radius, indicating that there is little spillover into regions close to the source. The *Reject Multiples* algorithm is closest to this ideal, followed by the *Second Highest Signal* and *Joint* algorithms. The *Maximum Signal Algorithm* has the highest contamination from misidentified Compton scatter events, and thus the largest spillover (evidenced by lower relative activities at each region radius).

V. Detectors Limited by Electronic Noise

A. Maximum Signal Algorithm

For N/S ratios <0.3 and ≤200 keV acceptance threshold, 22% of the events are misidentified when this algorithm is implemented (Figure 3a), rising slowly as the N/S ratio increases. As the acceptance threshold is increased, more events that deposit energy in multiple crystals are rejected, as the energy deposit is split between two crystals making it less likely that either crystal is above threshold. Thus, raising the threshold to 350 keV decreases the MIF to 14% but reduces the singles detection efficiency from 84% to 65% (Figure 3b). As we are unwilling to sacrifice sensitivity, 250 keV is the

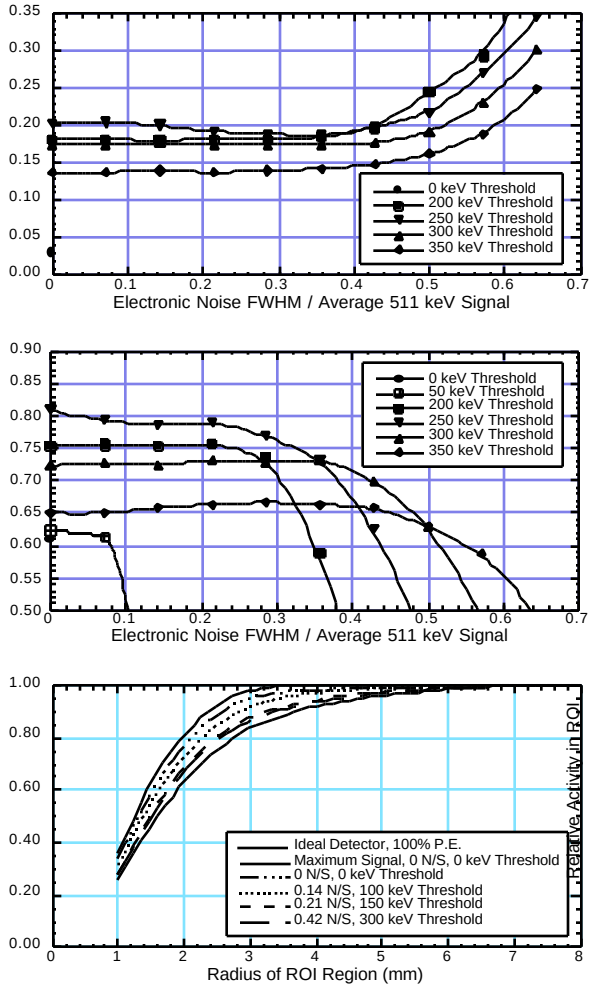

Figure 4: The (a) MIFs, (b) singles detection efficiency, and (c) relative activity in circular ROIs obtained with the *Reject Multiples* algorithm in detectors with energy resolution dominated by electrical noise.

highest practical threshold. This algorithm has good noise immunity, as the crystal with the highest true energy deposit is usually selected even in the presence of significant noise.

Figure 3c shows that for a N/S ratio for which this algorithm is appropriate (0.5), increasing the acceptance threshold increases the activity in small ROIs by reducing scatters and noisy channels and thus decreases the spillover into regions close to the source. While the improvement is slight, performance similar to the zero noise case is recovered with virtually no loss of sensitivity (*i.e.* at a 250 keV threshold). For this and all subsequent ROI plots, N/S values appropriate for the algorithm are selected.

B. Reject Multiples Algorithm

The dependence of the MIF and EFF on signal threshold is more pronounced in this algorithm than in the *Maximum Signal* algorithm. Low thresholds discard crystals with small signals (leaving only one signal where initially there were more), initially increasing both MIF and EFF (Figure 4), but increasing thresholds eventually give the expected decrease in both MIF and EFF. Only one value for the MIF and EFF at

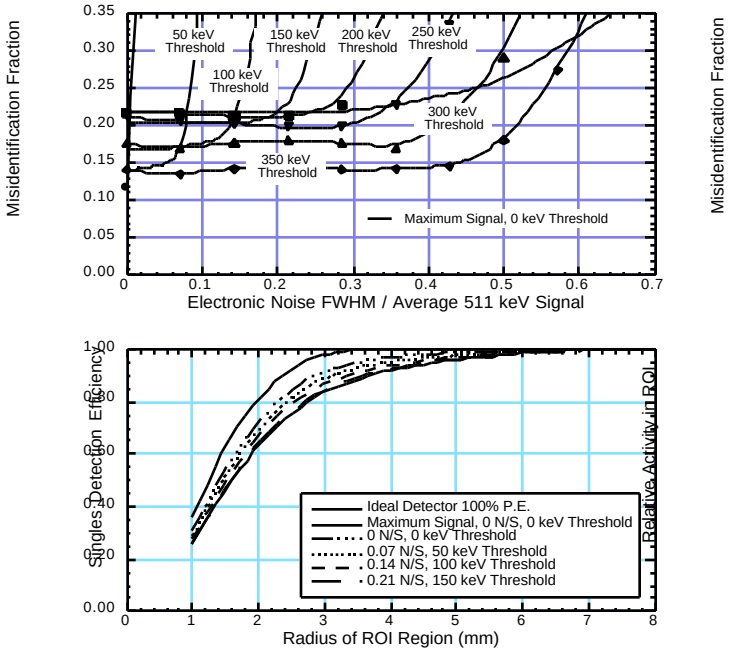

Figure 5: The (a) MIFs and (b) relative activity in circular ROIs obtained when the *Second Highest Signal* algorithm is implemented in detectors with energy resolution dominated by electrical noise.

zero threshold is displayed in Figure 4 because the algorithm (at this threshold) has vanishingly low efficiency with non-zero N/S ratios. For non-zero N/S ratios, this algorithm improves somewhat upon the *Maximum Signal* algorithm, but its efficiency degrades much faster as N/S increases. The 50 keV threshold curve in Figure 4b demonstrates how rapidly the efficiency degrades for small thresholds.

The ROI analysis for the *Reject Multiples* algorithm, shown in Figure 4c, demonstrates the improvement in quantitation possible by rejecting Compton scatter events. For Low N/S ratios, the ROI curves lie significantly above the *Maximum Signal* algorithm curve, and very close to the "perfect" detector curve (0 N/S, 100% photoelectric). The fraction of activity in a 2 mm ROI is increased from 62% (*Maximum Signal*) to nearly 80%.

C. Second Highest Signal Algorithm

For the *Second Highest Signal* algorithm to be effective, its threshold must be low enough that Compton scatters depositing energy in more than one crystal are considered (it is the forward, low energy deposit events that the algorithm has the best potential to identify) but not so low that photoelectric events (with noise in another channel) are compromised. The MIFs in Figure 5a show improvement over the *Maximum Signal* algorithm when N/S ratios are low (<0.2). For larger noise levels, thresholds >250 keV are required for effective operation, which leads to unacceptably low singles efficiency (the EFF of this algorithm is the same as the *Maximum Signal* algorithm, shown in Figure 3b). The ROI analysis for the *Second Highest Signal* algorithm, shown in Figure 5b, demonstrates that it has better quantitation than the *Maximum*

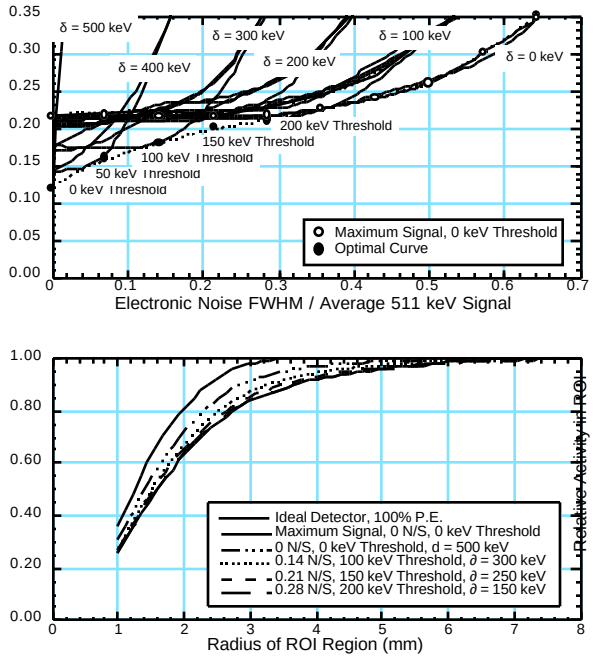

Figure 6: The (a) MIFs and (b) relative activity in circular ROIs obtained when the *Joint* algorithm is implemented in detectors with energy resolution dominated by electrical noise. In (a), for each value of δ there is a family of curves corresponding to different minimum energy thresholds. The boundary of these curves defines the Optimal Curve, and the minimum energy threshold at the optimum is noted for several N/S ratios.

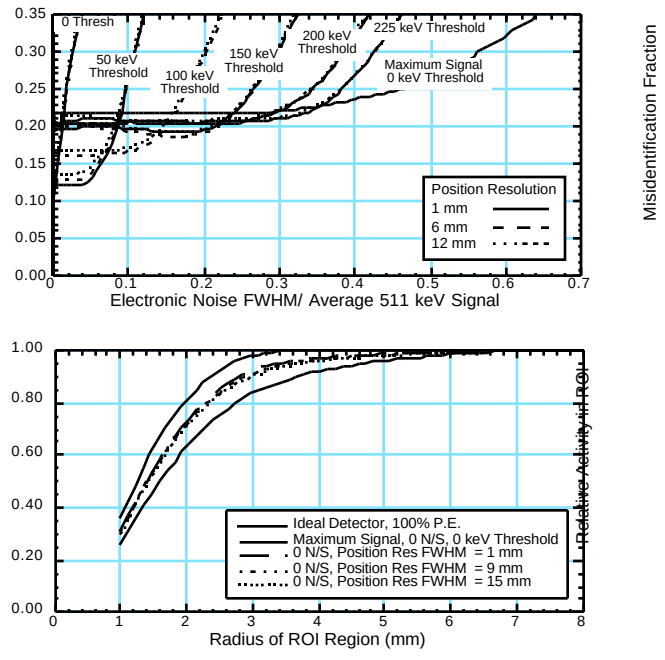

Figure 7: The (a) MIFs and (b) relative activity in circular ROIs obtained when the *Depth of Interaction* algorithm is implemented in detectors with energy resolution dominated by electrical noise. In (a) there is a family of curves corresponding to different DOI resolutions for each value of minimum energy threshold.

Signal algorithm, but not as good as the *Reject Multiples* algorithm. Overall, this algorithm has the best performance given a low, but non-zero, electronic noise.

D. Joint Algorithm

Figure 6a plots the MIF for the *Joint* algorithm. For each value of δ (the energy difference threshold), a family of curves is obtained as the minimum energy threshold is varied. For a given electronic noise, δ and the minimum energy threshold can be chosen for an "optimal" MIF — the dashed line in Figure 6a. For high N/S ratios, the optimal δ is small, forcing the algorithm to select the highest signal and making it equivalent to the *Maximum Signal* algorithm. For low N/S ratios, the optimal δ is large, forcing the algorithm to select the lowest signal and making it equivalent to the *Second Highest Signal* algorithm. When the N/S ratio is between 0.15 and 0.35, the optimal curve has a MIF as much as 3% lower than either the *Second Highest Signal* or the *Maximum Signal* algorithms for this "midrange" noise region. This algorithm uses the same event pool as the *Maximum Signal* and *Second Highest Signal* algorithms (whose EFF is given in Figure 3b) and all points on the "optimal curve" in Figure 6a have <250 keV minimum energy threshold, so all have 83%-84% singles efficiency. The ROI curves obtained with the *Joint* algorithm are shown in Figure 6b. As expected, the curve is similar to that for the *Second Highest Signal* algorithm for low N/S rations, while for high N/S ratios the results are similar to the *Maximum Signal* algorithm.

VI. Detectors with Depth of Interaction

Detector modules that measure depth of interaction (DOI) can use interaction positions to determine the crystal of first interaction. Interactions in Regions I and II in Figure 1 have a scattering angle θ<90°, so the crystal with energy deposit closest to the patient port is the crystal of first interaction in approximately 2/3 of the events with energy deposit in two crystals. This is true even for sources close to the edge of the patient port, as most Compton scatter is >30˚, which is the maximum incidence angle for a PET camera with a patient port half of the ring diameter. Thus, the *Depth of Interaction* algorithm selects the crystal with interaction depth closest to the patient port. If a crystal has no true energy deposit but noise fluctuations cause it to be a candidate crystal, a random DOI is assigned. Energy resolution is modeled as in Section V (dominated by electronic noise), but performance for detectors limited by counting statistics is the same as the zero noise results. Like the *Second Highest Signal* algorithm, this algorithm correctly identifies those events with energy deposit in a single crystal (70%), 2/3 of the events with energy deposit in two crystals (those in Compton kinematic Regions I & II, which comprise 16% of the events), and 3% from >2 crystal interactions, yielding a theoretical minimum MIF of 11%.

Figure 7a shows that for each energy threshold, a family of MIF curves is obtained as the DOI measurement resolution is varied. At each N/S ratio an "optimal" energy threshold can be obtained and an "optimal curve" can be drawn for each DOI measurement resolution, but is omitted to improve clarity. Improvement over the *Maximum Signal* algorithm is only

found at low N/S ratios, demonstrating the importance of correctly identifying Compton scatter. Even at low N/S ratios, the DOI measurement resolution has little affect on the MIF. This is partially because the mean length that a scattered photon travels before interacting is 1.1 cm (large compared to most DOI resolutions considered), and partly because randomly choosing a crystal of first interaction (which effectively happens with poor DOI resolution) has a theoretical minimum MIF of 16%, which is only slightly higher than the 11% theoretical minimum MIF for this algorithm.

This algorithm uses the same events as the *Maximum Signal*, *Second Highest Signal*, and *Joint* algorithms in Section V, so its EFF is described by Figure 3b. With perfect energy resolution, the ROI curves (Figure 7b) are similar to the *Second Highest Signal* algorithm (Figure 4c), which is expected as both algorithms correctly identify Compton scatters in the same kinematic regions (Regions I and II), and are nearly insensitive to DOI measurement resolution. At larger noise values (not shown in Figure 7b) the ROI curve approaches that of the *Maximum Signal* algorithm, and has even less dependence on DOI measurement resolution.

VII. Conclusions

We investigate algorithms to identify and correct for detector Compton scatter and improve the accuracy of the reconstructed image. Algorithms that *Reject Multiple* interactions decrease the MIF to 3%, but prohibitively degrade the EFF. For detectors with energy resolution limited by counting statistics, the *Maximum Signal* algorithm obtains a 22% MIF while the *Second Highest Signal* and *Joint* algorithms have a 12% MIF. For detectors with resolution limited by energy independent noise, the *Maximum Signal* algorithm has the best MIF when the N/S ratio is >0.35, with 22%–25% MIF for N/S ratios <0.5. The *Second Highest Signal* algorithm reduces the MIF to 12% but is only effective when the N/S ratio is <0.15. The *Joint* algorithm is the most versatile, as it is never worse than the *Maximum Signal* or *Second Highest Signal* algorithm (it mimics them for high and low N/S ratios respectively) and improves on them for intermediate N/S ratios. Detectors with the ability to measure the interaction position can reduce the MIF to 12%–15% depending on position resolution, but need low N/S ratios (similar to those for the *Second Highest Signal* algorithm) to be effective.

The effectiveness of any of the algorithms, even the *Depth of Interaction* algorithm, is critically dependent on correctly identifying crystals with energy deposit in them, and thus the energy resolution. Energy measurement error caused by counting statistics is much less problematic for this identification than error due to electronic noise because the greatest potential for improvement comes from correctly identifying events in kinematic Region I (unambiguous forward scatter), which has low (<175 keV) energy deposit in the crystal of first interaction. Since the RMS error caused by counting statistics fluctuations is smaller than the true energy, the absolute value of the energy error for these small energy deposits is also small. However, electronic noise errors are independent of the true energy, and so can be much larger than these small energy deposits, even for relatively small N/S ratios.

The effect of detector Compton scatter is virtually unobservable in the point spread function (fwhm or fwtm) and is often small in the ROI analysis. However, when the *Second Highest Signal* or the *Joint* algorithm has sufficiently low noise to be effective, there is significant (10%–20%) improvement in quantitation in regions <1 cm in diameter. This effect may be masked by patient Compton scatter when imaging humans, but may be significant in small animal (such as rodent) studies where the scatter fraction is lower. Tomographs specially designed for small animals are likely to have smaller crystal size (and ring diameter) than the geometry discussed here (3 mm square crystals in a 60 cm diameter ring), giving them the potential for higher spatial resolution but also making correction for Compton scatter with algorithms such as these significantly more important.

VIII. Acknowledgments

This work is supported in part by the Director, Office of Energy Research, Office of Health and Environmental Research, Medical Applications and Biophysical Research Division of the U.S. Department of Energy under contract No. DE-AC03-76SF00098, in part by the Public Health Service grants No. P01-HL25840 and No. R01-NS29655, awarded by the National Heart, Lung, and Blood Institute, and the Neurological Disorder and Stroke Institute, Department of Health and Human Services.

IX. References

[1] Lecomte R, Cadorette J, *et al.* Design and engineering aspects of a high resolution positron tomograph for small animal imaging. *IEEE Trans. Nucl. Sci.* NS–41: pp. 1446–1452, 1994.

[2] Moses WW, Derenzo SE, *et al.* Performance of a PET detector module utilizing an array of silicon photodiodes to identify the crystal of interaction. *IEEE Trans. Nucl. Sci.* NS-40: pp. 1036–1040, 1993.

[3] Cherry SR, Shao Y, *et al.* Collection of scintillation light from small BGO crystals. *IEEE Trans. Nucl. Sci.* NS-42: pp. 1058–1063, 1995.

[4] Cho ZH and Juh SC. Resolution and sensitivity improvement in positron emission tomography by the first interaction point determination. Proceedings of The IEEE 1991 Nuclear Science Symposium and Medical Imaging Conference, pp. 1623–1627, (Edited by G. Baldwin), Santa Fe, NM, 1991.

[5] Moses WW and Derenzo SE. Design studies for a PET detector module using a PIN photodiode to measure depth of interaction. *IEEE Trans. Nucl. Sci.* NS–41: pp. 1441–1445, 1994.

[6] Moisan C, Rogers JG, *et al.* Design studies of a depth encoding large aperture PET camera. *IEEE Trans. Nucl. Sci.* NS-42: pp. 1041–1050, 1995.

[7] Moses WW, Derenzo SE, *et al.* A room temperature LSO / PIN photodiode PET detector module that measures depth of interaction. *IEEE Trans. Nucl. Sci.* NS-42: pp. 1085–1089, 1995.